

Hidden Real Topology and Unusual Magnetoelectric Responses in Monolayer Antiferromagnetic Cr₂Se₂O

Jialin Gong,¹ Yang Wang,² Yilin Han,² Zhenxiang Cheng,³ Xiaotian Wang,^{1,3} Zhi-Ming Yu,² and Yugui Yao²

¹*School of Physical Science and Technology, Southwest University, Chongqing 400715, China*

²*Key Lab of advanced optoelectronic quantum architecture and measurement (MOE),*

Beijing Key Lab of Nanophotonics & Ultrafine Optoelectronic Systems,

and School of Physics, Beijing Institute of Technology, Beijing 100081, China

³*Institute for Superconducting and Electronic Materials (ISEM),*

University of Wollongong, Wollongong 2500, Australia

Recently, the real topology has been attracting widespread interest in two dimensions (2D). Here, based on first-principles calculations and theoretical analysis, we reveal the monolayer Cr₂Se₂O (ML-CrSeO) as the first material example of a 2D antiferromagnetic (AFM) real Chern insulator (RCI) with topologically protected corner states. Unlike previous RCIs, we find that the real topology of the ML-CrSeO is rooted in one certain mirror subsystem of the two spin channels, and can not be directly obtained from all the valence bands in each spin channel as commonly believed. In particular, due to antiferromagnetism, the corner modes in ML-CrSeO exhibit strong corner-contrasted spin polarization, leading to spin-corner coupling (SCC). This SCC enables a direct connection between spin space and real space. Consequently, large and switchable net magnetization can be induced in the ML-CrSeO nanodisk by electrostatic means, such as potential step and in-plane electric field, and the corresponding magnetoelectric responses behave like a sign function, distinguished from that of the conventional multiferroic materials. Our work considerably broadens the candidate range of RCI materials, and opens up a new direction for topo-spintronics and 2D AFM materials research.

Materials with nontrivial real band topology [1–4] have become a focus of current physics research. As a definition, the real topological phases feature real band eigenstates [1, 2], which can be guaranteed by certain symmetries, such as the presence of the spacetime inversion symmetry (\mathcal{PT}) and the absence of spin-orbit coupling (SOC) effect. Furthermore, for 2D systems both with and without SOC, the combined operator $C_{2z}\mathcal{T}$ (with z being the direction normal to the 2D plane) can also protect the real band topology [5, 6].

Various real topological phases are proposed in non-magnetic systems without SOC, including 2D and 3D RCIs, Z_2 nodal lines, Z_2 nodal surfaces, real Weyl and Dirac points [2, 6–18], and some of them have been experimentally realized [14–16]. Recently, Zhang *et al.* [18] demonstrated that the 2D RCI could also appear in ferromagnetic systems regardless of the SOC strength. However, the 2D RCI with AFM order has never been studied. Particularly, due to the magnetic but spin neutral property, one can expect that the AFM RCI may exhibit signatures distinct from the conventional and ferromagnetic RCIs, especially for the magnetoelectric responses [19, 20].

Generally, the real topology of a 2D insulator is characterized by a Z_2 real Chern number (also known as the second Stiefel-Whitney number) ν_R [1, 2], which can be evaluated from the eigenvalues of two-fold rotation C_{2z} or spatial inversion \mathcal{P} of the valence bands at the four C_{2z} (\mathcal{P}) invariant momentum points Γ_i ($i = 1, 2, 3, 4$) [2, 21]

$$(-1)^{\nu_R} = \prod_{i=1}^4 (-1)^{\lfloor n_{i,-}/2 \rfloor}, \quad (1)$$

where $\lfloor \dots \rfloor$ is the floor function, and $n_{i,-}$ is the number of valence states at four momentum points Γ_i which have negative eigenvalues. This formula (1) successfully predicts many RCI and topological Z_2 nodal line materials [6, 8, 10–18].

In this work, we show that there is a caveat for calculating ν_R of the system that can be divided into two or multiple *independent* subsystems, due to the floor function. For example, assuming the numbers of the valence states with negative C_{2z} eigenvalue in two independent subsystems are respectively $n_-^{(1)} = \{6, 6, 5, 4\}$, and $n_-^{(2)} = \{4, 4, 5, 6\}$ at the four C_{2z} -invariant points. For each subsystem, one can obtain a real Chern number by Eq. (1), which gives $\nu_R^{(1)} = 0$ and $\nu_R^{(2)} = 1$. Therefore, the whole system is topologically nontrivial. However, this real topology is missed if one directly applies Eq. (1) to the whole system, as $n_- = n_-^{(1)} + n_-^{(2)} = \{10, 10, 10, 10\}$, which gives a trivial real Chern number $\nu_R = 0$. This simple case tells us that for the materials hosting multiple independent subsystems, since Eq. (1) does not naturally guarantee $\nu_R = \sum_i \nu_R^{(i)} \bmod 2$ (with $\nu_R^{(i)}$ denoting the real Chern number of the i -th subsystem), the real topology of the whole system may be hidden in one certain subsystem, and needs to be carefully examined.

Via first-principles calculations and theoretical analysis, we demonstrate the aforementioned hidden real topology in ML-CrSeO, which has a horizontal mirror M_z , and then two independent mirror subsystems. Particularly, the ground state of the ML-CrSeO exhibits out-of-plane intralayer AFM order. This means that the ML-CrSeO is also the first material example of a 2D

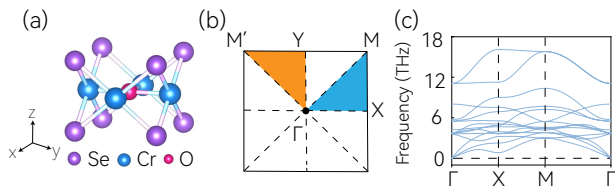


FIG. 1. (a) Side view of the crystalline structure of ML-CrSeO. (b) The first Brillouin zone (BZ) of ML-CrSeO. The orange and blue regions are the two irreducible parts of the first BZ. (c) Calculated phonon spectrum of ML-CrSeO.

AFM RCI. Compared with the previously reported non-magnetic and ferromagnetic RCIs [6, 8, 11, 13, 17, 18], the topological corner states in ML-CrSeO are spin-polarized, however, the direction of the spin polarization is corner-dependent, leading to a unique SCC effect in 2D AFM RCIs. The SCC can be directly observed by spin-resolved scanning tunneling spectroscopy (STS) [22]. Furthermore, it can fundamentally affect the magnetoelectric responses of the systems. We find that by applying electrostatic fields, the net magnetization of the ML-CrSeO can be efficiently changed from zero to a finite constant. Remarkably, the sign of the finite constant is solely determined by the direction of the electrostatic fields, and is switched when changing the direction of the fields. Hence, the magnetoelectric responses in ML-CrSeO behave as a sign function, distinguished from those in the conventional multiferroic materials [23] and the previously reported RCIs. This sign-function response also indicates an electric switching of the net magnetization in ML-CrSeO, which is important for device applications [24–26].

Structure and magnetic ordering.— The ML-CrSeO is a kind of oxyseLENides. The crystal structure of the ML-CrSeO is shown in Fig. 1(a), in which three atomic sublayers with two Cr and one O atoms as the middle layer and two Se atoms as the upper and lower layers are obvious. The crystal lattice has space group (SG) P4/mmm (No. 123), which preserves C_{4z} , C_{2x} and M_z symmetries. The optimized lattice constant is calculated as $a = b = 4.02$ Å. We also find that the ML-CrSeO is both dynamically and thermodynamically stable, as shown in Fig. 1(c) and the supplemental material (SM) [27].

Since the ML-CrSeO has transition metal elements, one can expect that it may exhibit magnetic ordering in its ground state. Our calculations show each Cr atom indeed has a finite magnetic moment, which is obtained as $\sim 3.1 \mu_B$. By comparing the energies of several typical types of magnetic ordering [27], we find that the ground state of ML-CrSeO is a C-type AFM with intralayer out-of-plane magnetization, i.e., the two Cr atoms in the unit cell have opposite spin polarization, as shown in Fig. 2(b). With magnetic ordering, the ML-CrSeO belongs to magnetic SG No. 123.342, which keeps $C_{4z}\mathcal{T}$, C_{2z} and M_z

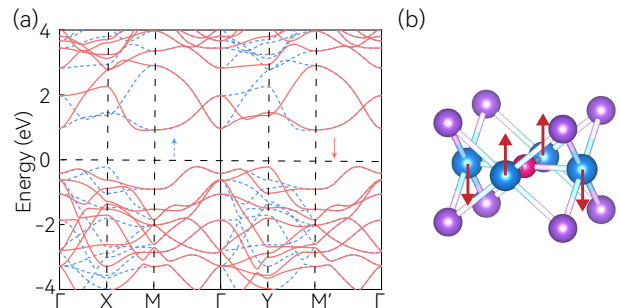


FIG. 2. (a) Spin-resolved band structures for ML-CrSeO without SOC. (b) The ground state of the ML-CrSeO, which is a intralayer out-of-plane (C-type) AFM.

symmetries, but breaks both C_{4z} and \mathcal{T} [28–30]. The combined operator $C_{4z}\mathcal{T}$ guarantees the spin neutrality of the monolayer.

Electronic band and hidden real topology.— We then investigate the electronic band structure of the ML-CrSeO with the AFM ground state. Since the SOC effect is rather small in the ML-CrSeO [27], we focus on the band structure without SOC.

When SOC is neglected, the two spin channels of the ML-CrSeO are decoupled but not independent, as they are connected by $C_{4z}\mathcal{T}$. Each spin channel can be regarded as an effective spinless system persevering \mathcal{T} . Obviously, each spin channel does not have C_{4z} symmetry and then the crystal symmetry of SG 123. By detailed analysis, we find that it is the crystal symmetry of SG 47 that is respected by each spin channel. The generators of SG 47 are C_{2x} , C_{2z} and M_z . Hence, the Hamiltonian of the ML-CrSeO (without SOC) can be written as

$$\mathcal{H} = \mathcal{H}_\uparrow \oplus \mathcal{H}_\downarrow = \mathcal{H}_0 \oplus C_{4z}\mathcal{H}_0C_{4z}^{-1}, \quad (2)$$

where \mathcal{H}_0 denotes a spinless and nonmagnetic Hamiltonian respecting the symmetry of SG 47. Since \mathcal{H}_0 has C_{2x} and \mathcal{T} , one knows that the two spin channels should be degenerate along Γ -M path.

The spin-resolved band structures for the ML-CrSeO are shown in Fig. 2(a), in which the spin-up and spin-down bands are degenerate on the high-symmetry line Γ -M (M'), consistent with the above symmetry analysis. Besides, the spin-up and spin-down bands are split at other momenta in BZ. Recently, the systems with spin-splitting band structures are also termed as altermagnetic

TABLE I. C_{2z} eigenvalues of all occupied bands at Γ , X, Y, and M points of the ML-CrSeO.

	Spin-up				Spin-down				
	Γ	X	Y	M	Γ	X	Y	M	
n_+	10	10	11	11	n_+	10	11	10	11
n_-	11	11	10	10	n_-	11	10	11	10
	$\nu_R = 0$				$\nu_R = 0$				

TABLE II. Mirror-resolved C_{2z} eigenvalues of all occupied bands at Γ , X, Y, and M points of the ML-CrSeO. Both spin channels are considered.

	Spin-up				Spin-down												
	$M_z = 1$				$M_z = -1$												
	Γ	X	Y	M	Γ	X	Y	M	Γ	X	Y	M					
n_+	5	6	8	7	5	4	3	4	n_+	5	8	6	7				
n_-	8	7	5	6	3	4	5	4	n_-	8	5	7	6				
	$\nu_R = 0$				$\nu_R = 1$					$\nu_R = 0$				$\nu_R = 1$			

materials [31–36]. For both spin channels, large gaps of 1.12 eV appear. Then, we can define a real Chern number ν_R^σ (with $\sigma = \uparrow, \downarrow$) for each spin subspace, as it preserves both C_{2z} and \mathcal{T} symmetries. Since C_{4z} commutes with C_{2z} , one always has $\nu_R^\uparrow = \nu_R^\downarrow$. The results of the C_{2z} eigenvalues of valence bands at the four C_{2z} -invariant momentum points are listed in Table I. Obviously, according to Eq. (1), both spin channels are topologically trivial with $\nu_R^\uparrow = \nu_R^\downarrow = 0$. However, as aforementioned, this result may not be correct if the spin channels can be further divided into independent subsystems.

The ML-CrSeO is exactly the case, as it has a horizontal mirror M_z and then can be divided into two independent subsystems based on the eigenvalue of M_z , i.e.,

$$\mathcal{H}_{\uparrow(\downarrow)} = \mathcal{H}_{\uparrow(\downarrow)}^+ \oplus \mathcal{H}_{\uparrow(\downarrow)}^-, \quad (3)$$

where $\mathcal{H}_{\uparrow(\downarrow)}^\pm$ denotes the subsystem with $M_z = \pm 1$ of spin-up (spin-down) channel. All the mirror subsystems also have both C_{2z} and \mathcal{T} . By analysing the mirror eigenvalue of the bands in each spin channel, we obtain a mirror-resolved band structure for the ML-CrSeO [see Fig. 3(a)]. For each mirror subsystem, we count the bands with negative C_{2z} eigenvalue, and the result is listed in Table II. Using Eq. (1), we find that for both spin-up and spin-down channels, the mirror subsystem with $M_z = -1$ has a nontrivial $\nu_R^- = 1$, while the $M_z = 1$ subsystem is trivial with $\nu_R^+ = 0$. Consequently, the *exact* real Chern number for each spin channel is $\nu_R^\uparrow = \nu_R^\downarrow = \nu_R^+ + \nu_R^- = 1$. This confirms that the ML-CrSeO is a material candidate for AFM RCI with hidden real topology.

Corner states and spin-corner coupling.— According to the bulk-boundary correspondence, the nontrivial real Chern number $\nu_R^- = 1$ will lead to protected corner states on a pair of C_{2z} -related intersections in each spin channel, and the corner states should have a mirror eigenvalue of $M_z = -1$. Moreover, since the spin-up and spin-down channels are connected by $C_{4z}\mathcal{T}$, there genetically exhibit four corner states as a group in the bulk band gap: two from spin-up channels and two from spin-down channels.

To demonstrate this feature, a wannier tight-binding model for a quadrangle nanodisk composed of 64 unit cells was constructed based on the ML-CrSeO with the preservation of $C_{4z}\mathcal{T}$ symmetry, as shown in Fig. 3(d). The obtained discrete energy spectrum of the quadrangle

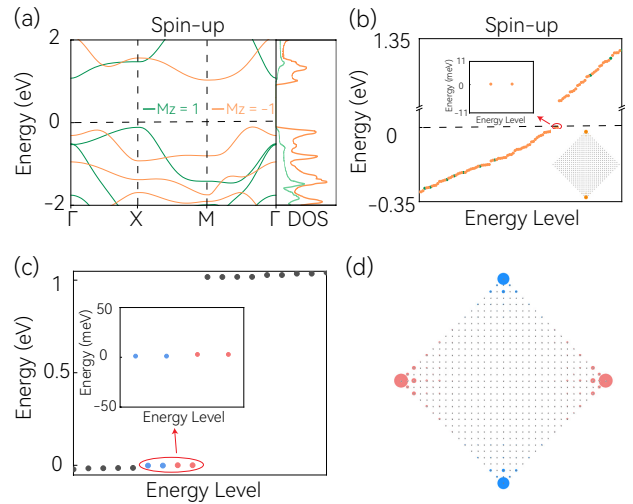


FIG. 3. (a) Mirror-resolved band structure and density of states (DOS) of the spin-up channel of the ML-CrSeO. The spin-down channel has a similar band structure, as the two spin channels are connected by $C_{4z}\mathcal{T}$ symmetry. (b) Mirror-resolved energy spectrum for the spin-up channel on a quadrangle-shaped disk. Orange and green curves and dots in (a) and (b) denote the states with $M_z = -1$ and $M_z = 1$, respectively. We also plot the spectrum and the spatial charge distribution of the corner states as insets in (b). (c) The energy spectrum for the whole ML-CrSeO on a quadrangle-shaped disk, where four corner states (the colored dots) as a group can be observed. (d) Spatial distribution of the corner states. The blue and red dots (circles) in (c) [(d)] correspond to the spin-up and spin-down corner states, respectively.

nanodisk is plotted in Fig. 3(c), in which four degenerate states in the bulk band gap are observed. By analysing the wave function of the four states, we confirm that they are indeed corner states, as they are localized at the four corners of the disk [see Fig. 3(d)]. Moreover, all these corner states are from the $M_z = -1$ subsystems [see Fig. 3(b)] and are fully spin polarized, as the SOC effect is neglected during the calculations. We would like to point out that both the existence and the spin polarization of the corner states are robust against the SOC effect [27].

Remarkably, the corner states at x -axis (labelled as X corner) are spin-down, whereas those at y -axis (labelled as Y corner) are spin-up, as shown in Fig. 3(d). This corner-contrasted spin polarization directly couples the

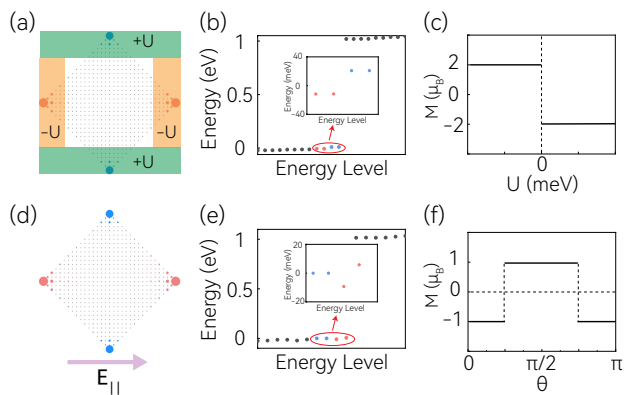


FIG. 4. SCC-induced electric control of the magnetization. (a) Schematic figure showing potential-step control of the magnetization of the ML-CrSeO disk. (b) The energy spectrum for the ML-CrSeO disk under a potential step $U = 0.01$ eV. (c) Net magnetization as a function of U . (d) With corner-dependent spin polarization, an in-plane electric field can lead to net magnetization in the ML-CrSeO disk. (e) The energy spectrum for the ML-CrSeO disk under an electric field of $E_x = 0.00025$ eV/Å, corresponding to $\theta = 0$. (f) Net magnetization as a function of θ . The blue and red circles (dots) are spin-up and spin-down corner states.

real space and spin space, leading to a novel SCC effect. Since the corner states are well separated in real space (for example, the distance between every two corners in Fig. 3(d) is larger than 3.2 nm), this provides great convenience for experimentally controlling the spins at each corner independently. Moreover, as electronic states at the Fermi level play a key role in many material properties, the independent control of the spin in each corner is expected to exhibit distinctive signatures.

Novel magnetoelectric responses.— We then investigate the magnetoelectric responses in the ML-CrSeO. A unique feature of AFM materials is that it is magnetic but spin-neutral [37, 38]. This provides an ideal platform for generating net magnetization and spin current by nonmagnetic methods. As studied in previous works [19, 20, 39–42], these novel magnetoelectric responses generally require certain bulk band structures like spin-layer coupling [20] and C-paired spin-valley locking [19], which, however, are absent in the ML-CrSeO.

In contrast, we investigate the magnetoelectric responses of a ML-CrSeO nanodisk with a novel SCC effect. While the corner states in ML-CrSeO are fully spin polarized, the nanodisk does not have net magnetization as guaranteed by the $C_{4z}\mathcal{T}$ symmetry. Hence, by breaking the $C_{4z}\mathcal{T}$, the ML-CrSeO nanodisk generally has finite net magnetization. There are many nonmagnetic ways to realize this symmetry breaking, such as uniaxial strain, applying nonmagnetic substrate without C_{4z} symmetry and interface engineering. Among them, the electrostatic means may be the most convenient in experiments and applications [43]. Here, we propose two

electrostatic means to achieve net magnetization in the ML-CrSeO nanodisk.

As the four corners of the nanodisk are well separated, we can apply a potential step to make each corner to have different potential energy. Specifically, we assume that the potential step satisfies $V = -U$ for the X corners and $V = +U$ for the Y corners, as illustrated in Fig. 4(a). The calculated spectrum of the nanodisk with $U = 0.01$ eV is shown in Fig. 4(b). As expected, the degenerate of the X and Y corners is broken. The Y (X) corners increase (decrease) in energy, but the bulk states are less affected. Hence, with half doping of the corner states, only the X corners are occupied, and then the net magnetization of the system is $M = -2\mu_B$. Moreover, the net magnetization can be switched by reversing the value of U . Consequently, the net magnetization takes the form of a sign function by varying the electrostatic potential, as shown in Fig. 4(c).

We can also use in-plane electric field $\mathbf{E}_{\parallel} = \{E \cos \theta, E \sin \theta\}$ to produce a corner-dependent electrostatic potential [see Fig. 4(d)]. When the electric field is along the x -direction ($\theta = 0$), the four corner states are split into three groups in energy: the -X (+X) corner has the lowest (highest) energy, while the two Y corners are in the middle [see Fig. 4(e)]. Then, with 1/4 doping of the corner states, only the -X corner is occupied, and then the net magnetization of the system is $M = -1\mu_B$. Similarly, if $\theta = \pi/2$, one would have $M = 1\mu_B$. Our detailed calculations show that the net magnetization has a sign-function dependence on the rotation angle of the electric field, as shown in Fig. 4(f). These sign functions of the magnetoelectric responses are completely different from the conventional magnetoelectric responses, suggesting the potential of the AFM RCIs for novel device operations.

Discussion.— In this work, we have unveiled a hidden real topology in a 2D AFM material with mirror symmetry. The underlying physics is to study the real topology in each independent subsystem, rather than the whole system. We then predict the ML-CrSeO as the first material example of the AFM RCI with hidden real topology. We also show that the 2D AFM RCI exhibits the SCC effect, which enables a direct control of the net magnetization of the system by both local and global electric methods.

Besides the ML-CrSeO, we find six other 2D AFM materials, including Cr_2Br_2 , Mn_2Br_2 , V_2Br_2 , Mn_2F_2 , Cr_2Cl_2 , and $\text{V}_2\text{Se}_2\text{O}$ as the AFM RCIs with hidden real topology [27]. Interestingly, the Cr_2Br_2 , Cr_2Cl_2 , and $\text{V}_2\text{Se}_2\text{O}$ are also valleytronics materials [44–47] with two valleys located at X and Y points in the BZ. Last but not least, it is necessary to re-examine the previous 2D materials with a horizontal mirror. With the hidden real topology proposed here, one can expect that many candidates previously diagnosed as trivial may have a non-trivial real Chern number.

-
- [1] Y. X. Zhao and Y. Lu, *Physical Review Letters* **118**, 056401 (2017).
- [2] J. Ahn, D. Kim, Y. Kim, and B.-J. Yang, *Physical Review Letters* **121**, 106403 (2018).
- [3] Q. Wu, A. A. Soluyanov, and T. Bzdušek, *Science* **365**, 1273 (2019).
- [4] A. Luo, Z. Song, and G. Xu, *npj Computational Materials* **8**, 26 (2022).
- [5] J. Ahn and B.-J. Yang, *Physical Review B* **99**, 235125 (2019).
- [6] J. Zhu, W. Wu, J. Zhao, C. Chen, Q. Wang, X.-L. Sheng, L. Zhang, Y. X. Zhao, and S. A. Yang, *Physical Review B* **105**, 085123 (2022).
- [7] W. Wu, Y. Liu, S. Li, C. Zhong, Z.-M. Yu, X.-L. Sheng, Y. X. Zhao, and S. A. Yang, *Physical Review B* **97**, 115125 (2018).
- [8] X.-L. Sheng, C. Chen, H. Liu, Z. Chen, Z.-M. Yu, Y. X. Zhao, and S. A. Yang, *Physical Review Letters* **123**, 256402 (2019).
- [9] Y. Zhao, *Frontiers of Physics* **15**, 1 (2020).
- [10] K. Wang, J.-X. Dai, L. B. Shao, S. A. Yang, and Y. X. Zhao, *Physical Review Letters* **125**, 126403 (2020).
- [11] C. Chen, W. Wu, Z.-M. Yu, Z. Chen, Y. X. Zhao, X.-L. Sheng, and S. A. Yang, *Physical Review B* **104**, 085205 (2021).
- [12] C. Chen, X.-T. Zeng, Z. Chen, Y. X. Zhao, X.-L. Sheng, and S. A. Yang, *Physical Review Letters* **128**, 026405 (2022).
- [13] M. Pan, D. Li, J. Fan, and H. Huang, *npj Comput. Mater.* **8**, 1 (2022).
- [14] Y. Pan, C. Cui, Q. Chen, F. Chen, L. Zhang, Y. Ren, N. Han, W. Li, X. Li, Z.-M. Yu, *et al.*, *Nature Communications* **14**, 6636 (2023).
- [15] H. Xue, Z. Chen, Z. Cheng, J. Dai, Y. Long, Y. Zhao, and B. Zhang, *arXiv preprint arXiv:2304.06304* (2023).
- [16] X. Xiang, X. Ni, F. Gao, X. Wu, Z. Chen, Y.-G. Peng, and X.-F. Zhu, *arXiv preprint arXiv:2304.12735* (2023).
- [17] J. Li, Y. Liu, J. Bai, C. Xie, H. Yuan, Z. Cheng, W. Wang, X. Wang, and G. Zhang, *Applied Physical Review* **10**, 031416 (2023).
- [18] X. Zhang, T. He, Y. Liu, X. Dai, G. Liu, C. Chen, W. Wu, J. Zhu, and S. A. Yang, *Nano Letters* **23**, 7358 (2023).
- [19] H.-Y. Ma, M. Hu, N. Li, J. Liu, W. Yao, J.-F. Jia, and J. Liu, *Nature Communications* **12**, 2846 (2021).
- [20] R.-W. Zhang, C. Cui, R. Li, J. Duan, L. Li, Z.-M. Yu, and Y. Yao, *arXiv preprint arXiv:2306.08902* (2023).
- [21] J. Ahn, S. Park, D. Kim, Y. Kim, and B.-J. Yang, *Chinese Physics B* **28**, 117101 (2019).
- [22] R. Wiesendanger, *Reviews of Modern Physics* **81**, 1495 (2009).
- [23] W. Eerenstein, N. Mathur, and J. F. Scott, *Nature* **442**, 759 (2006).
- [24] F. Matsukura, Y. Tokura, and H. Ohno, *Nature Nanotechnology* **10**, 209 (2015).
- [25] P. Wadley, B. Howells, J. Železný, C. Andrews, V. Hills, R. P. Campion, V. Novák, K. Olejník, F. Maccherozzi, S. Dhesi, *et al.*, *Science* **351**, 587 (2016).
- [26] C. Song, B. Cui, F. Li, X. Zhou, and F. Pan, *Progress in Materials Science* **87**, 33 (2017).
- [27] See Supplemental Material (SM) for the computational methods, Monte Carlo simulations of temperature-dependent magnetization, spin-orbit coupling effect, and other AFM RCIs with hidden real topology, etc.
- [28] G.-B. Liu, Z. Zhang, Z.-M. Yu, S. A. Yang, and Y. Yao, *Phys. Rev. B* **105**, 085117 (2022).
- [29] Z.-M. Yu, Z. Zhang, G.-B. Liu, W. Wu, X.-P. Li, R.-W. Zhang, S. A. Yang, and Y. Yao, *Science Bulletin* **67**, 375 (2022).
- [30] Z. Zhang, G.-B. Liu, Z.-M. Yu, S. A. Yang, and Y. Yao, *Phys. Rev. B* **105**, 104426 (2022).
- [31] L. Šmejkal, J. Sinova, and T. Jungwirth, *Physical Review X* **12**, 040501 (2022).
- [32] Z. Feng, X. Zhou, L. Šmejkal, L. Wu, Z. Zhu, H. Guo, R. González-Hernández, X. Wang, H. Yan, P. Qin, *et al.*, *Nature Electronics* **5**, 735 (2022).
- [33] L. Šmejkal, A. H. MacDonald, J. Sinova, S. Nakatsuji, and T. Jungwirth, *Nature Reviews Materials* **7**, 482 (2022).
- [34] L. Šmejkal, J. Sinova, and T. Jungwirth, *Physical Review X* **12**, 031042 (2022).
- [35] H. Bai, Y. C. Zhang, Y. J. Zhou, P. Chen, C. H. Wan, L. Han, W. X. Zhu, S. X. Liang, Y. C. Su, X. F. Han, F. Pan, and C. Song, *Physical Review Letters* **130**, 216701 (2023).
- [36] J. A. Ouassou, A. Brataas, and J. Linder, *Physical Review Letters* **131**, 076003 (2023).
- [37] V. Baltz, A. Manchon, M. Tsoi, T. Moriyama, T. Ono, and Y. Tserkovnyak, *Reviews of Modern Physics* **90**, 015005 (2018).
- [38] H. Yan, Z. Feng, P. Qin, X. Zhou, H. Guo, X. Wang, H. Chen, X. Zhang, H. Wu, C. Jiang, *et al.*, *Advanced Materials* **32**, 1905603 (2020).
- [39] L. Šmejkal, J. Železný, J. Sinova, and T. Jungwirth, *Phys. Rev. Lett.* **118**, 106402 (2017).
- [40] D.-F. Shao, S.-H. Zhang, M. Li, C.-B. Eom, and E. Y. Tsymbal, *Nature Communications* **12**, 7061 (2021).
- [41] R. González-Hernández, L. Šmejkal, K. Výborný, Y. Yahagi, J. Sinova, T. c. v. Jungwirth, and J. Železný, *Phys. Rev. Lett.* **126**, 127701 (2021).
- [42] D.-F. Shao, Y.-Y. Jiang, J. Ding, S.-H. Zhang, Z.-A. Wang, R.-C. Xiao, G. Gurung, W. J. Lu, Y. P. Sun, and E. Y. Tsymbal, *Phys. Rev. Lett.* **130**, 216702 (2023).
- [43] Z.-M. Yu, S. Guan, X.-L. Sheng, W. Gao, and S. A. Yang, *Phys. Rev. Lett.* **124**, 037701 (2020).
- [44] J. R. Schaibley, H. Yu, G. Clark, P. Rivera, J. S. Ross, K. L. Seyler, W. Yao, and X. Xu, *Nature Reviews Materials* **1**, 1 (2016).
- [45] L. Li, M. Wu, and X. C. Zeng, *Advanced Functional Materials* **29**, 1905752 (2019).
- [46] J. Chu, Y. Wang, X. Wang, K. Hu, G. Rao, C. Gong, C. Wu, H. Hong, X. Wang, K. Liu, *et al.*, *Advanced Materials* **33**, 2004469 (2021).
- [47] Y. Liu, Y. Feng, T. Zhang, Z. He, Y. Dai, B. Huang, and Y. Ma, *Advanced Functional Materials* , 2305130 (2023).